Structural and geochemical characteristics of faulted sediments and inferences on the role of water in deformation, Rio Grande Rift, New Mexico

Jonathan Saul Caine[†] **and Scott A. Minor**
U.S. Geological Survey, P.O. Box 25046, MS 964, Denver, Colorado 80225, USA

ABSTRACT

The San Ysidro fault is a spectacularly exposed normal fault located in the northwestern Albuquerque Basin of the Rio Grande Rift. This intrabasin fault is representative of many faults that formed in poorly lithified sediments throughout the rift. The fault is exposed over nearly 10 km and accommodates nearly 700 m of dip slip in subhorizontal, siliciclastic sediments. The extent of the exposure facilitates study of along-strike variations in deformation mechanisms, architecture, geochemistry, and permeability. The fault is composed of structural and hydrogeologic components that include a clay-rich fault core, a calcite-cemented mixed zone, and a poorly developed damage zone primarily consisting of deformation bands. Structural textures suggest that initial deformation in the fault occurred at low temperature and pressure, was within the paleosaturated zone of the evolving Rio Grande Rift, and was dominated by particulate flow. Little geochemical change is apparent across the fault zone other than due to secondary processes. The lack of fault-related geochemical change is interpreted to reflect the fundamental nature of water-saturated, particulate flow. Early mechanical entrainment of low-permeability clays into the fault core likely caused damming of groundwater flow on the up-gradient, footwall side of the fault. This may have caused a pressure gradient and flow of calcite-saturated waters in higher-permeability, fault-entrained siliciclastic sediments, ultimately promoting their cementation by sparry calcite. Once developed, the cemented and clay-rich fault has likely been, and continues to be, a partial barrier to cross-fault groundwater flow, as suggested by petrophysical measurements. Aeromagnetic data indicate that there may be many more unmapped faults with similar lengths to the San Ysidro fault buried within Rio Grande basins. If these buried faults formed by the same processes that formed the San Ysidro fault and have persistent low-permeability cores and cemented mixed zones, they could compartmentalize the basin-fill aquifers more than is currently realized, particularly if pumping stresses continue to increase in response to population growth.

INTRODUCTION

Although it is commonly known that fault zones are mechanical and hydrologic heterogeneities in Earth's upper crust (e.g., Lovering, 1942; Sibson, 1977; Chester and Logan, 1986; McCaig, 1989; Bruhn et al., 1990; Martel, 1990; Knipe, 1993; Antonellini and Aydin, 1994; Sibson, 1994; Haneberg, 1995; Caine et al., 1996; Lopez and Smith, 1996; Hitzman, 1999; Shipton et al., 2002; Wibberley et al., 2008), the internal properties that cause heterogeneity, their three-dimensional variations, and the fundamental processes that lead to these variations are poorly understood. The purpose of this paper is to add to the growing body of literature that focuses on the characteristics of fault zones in poorly lithified, siliciclastic sediments, with particular emphasis on the fault core, where a significant amount of strain is accommodated. Such fault zones are distinct from their counterparts in well-lithified sedimentary rock (e.g., Heynekamp et al., 1999; Rawling et al., 2001; Bense et al., 2003), and the San Ysidro fault zone in the middle Rio Grande Rift of New Mexico is an exceptionally well-exposed example. In this paper, we present the results of detailed structural, lithologic, geochemical, and petrophysical analyses and observations from several locations along a 10-km-strike exposure of the San Ysidro fault zone. Using these data, we characterize the macroscopic form of the fault zone and infer the key deformation mechanisms that formed it. We also speculate on the deformation conditions and present textural and geochemical evidence that water played an important role in the formation of the fault zone.

Our hypothesis is that in its initial stages of growth, prior to partial lithification and fault-localized calcite cementation, the San Ysidro fault formed at low temperature and shallow depth by particulate flow in the saturated zone of a paleo–groundwater-flow system. Although common to the formation of many fault zones in the brittle crust, clay-rich fault cores appear to evolve by different processes due to differences in protolith composition, water saturation, and degree of lithification (cf. Engelder, 1974; Lindsay et al., 1993; Vrolijk and van der Pluijm, 1999; Rawling and Goodwin, 2003, 2006). Our results highlight the importance of mechanical versus geochemical processes in the formation of clay-rich fault cores in dominantly siliciclastic, poorly lithified sediments.

The San Ysidro fault was originally selected to study the origins of linear anomalies revealed in high-resolution aeromagnetic data acquired over the Albuquerque Basin and interpreted as intrabasin faults by Grauch et al. (2001). Our studies of exposures of aeromagnetically resolved faults, such as the San Ysidro, have shown that the anomalies are caused by juxtaposition of subhorizontally layered Santa Fe Group sediments with varying concentrations of magnetic minerals (Grauch et al., 2006; Hudson et al., 2008). On the basis of this work, we propose that the San Ysidro fault may be an analog for buried, aeromagnetically resolved, rift basin faults in general. We also discuss the role of this class of faults in the potential compartmentalization of the Santa Fe Group aquifer system due to their exceptionally persistent, low permeability, clay-rich fault cores and calcite-cemented mixed zones (cf. Minor and Hudson, 2006).

REGIONAL GEOLOGIC SETTING

The San Ysidro fault is located in the northwestern Albuquerque Basin (Fig. 1). The Albuquerque Basin is one of numerous basins of the

[†]E-mail: jscaine@usgs.gov

GSA Bulletin; September/October 2009; v. 121; no. 9/10; p. 1325–1340; doi: 10.1130/B26164.1; 11 figures; Data Repository item 2009132.

Rio Grande Rift in Colorado and New Mexico (May and Russell, 1994; Minor and Hudson, 2006). The basin initiated its formation during the early Miocene and is still evolving (Kelley, 1982; Chapin and Cather, 1994). The Albuquerque Basin has been syntectonically filled with Santa Fe Group fluvial, debris-flow, eolian, and playa sediments. These are primarily derived from Proterozoic through Cenozoic bedrock exposed in the nearby rift flanks, as well as sediment transported into the basin via the ancestral Rio Grande drainage system (Connell et al., 1999; Smith et al., 2001).

Siliciclastic sands, silts, and gravels dominate the basin-fill sediments in the vicinity of the San Ysidro fault. Several distinctly pure and laterally extensive clay units, which are each generally not more than 1 to 2 m thick, also are present in the section. Numerous gravel-rich beds are compositionally immature, and high percentages of pebbles and cobbles are derived from the Jemez volcanic field to the north and Proterozoic metamorphic rocks of the Sangre de Cristo Mountains to the northeast (Fig. 1). Santa Fe Group sediments typically are highly friable, reflecting their poor degree of lithification due to their recent, rapid deposition and generally shallow burial. Calcite cementation is variably found throughout the sedimentary section and is sometimes localized in fault zones (Mozley and Goodwin, 1995; Heynekamp et al., 1999; Mozley et al., 2004; Minor and Hudson, 2006). Meters beyond the fault zone, several sandy units show strata-parallel or strata-bound cement that commonly forms curb-and-gutter–like structures and subhorizontal shelf-like features that are resistant to erosion. Collectively, Santa Fe Group sediments form generally flat-lying aquifer and aquitard units, from which the bourgeoning population of the region gets its groundwater (Hawley et al., 1995).

The thickness of the northern Albuquerque Basin fill sediments ranges from <250 m to 4300 m, and the approximate thickness is 1200 m in the vicinity of the San Ysidro fault (May and Russell, 1994; Grauch et al., 1999; Minor and Hudson, 2006). On the basis of minimum sediment thicknesses and exposed unconformities reported in Koning et al. (1998) and Connell et al. (1999), we can make estimates regarding the exhumation, and thus minimum burial, of sediments now exposed along the San Ysidro fault. The sediments in our study area have been exhumed from paleodepths ranging from at least 750 m to 1050 m in the footwall and 15 m (essentially the paleo–ground surface) to 770 m in the hanging wall. Thickening of hanging wall relative to footwall units, observed throughout the Albuquerque Basin, is indicative of growth faulting (Chapin and Cather, 1994; May and Russell, 1994; Connell et al., 1999; Smith et al., 2001; Minor and Hudson, 2006), making definitive estimates of maximum burial difficult.

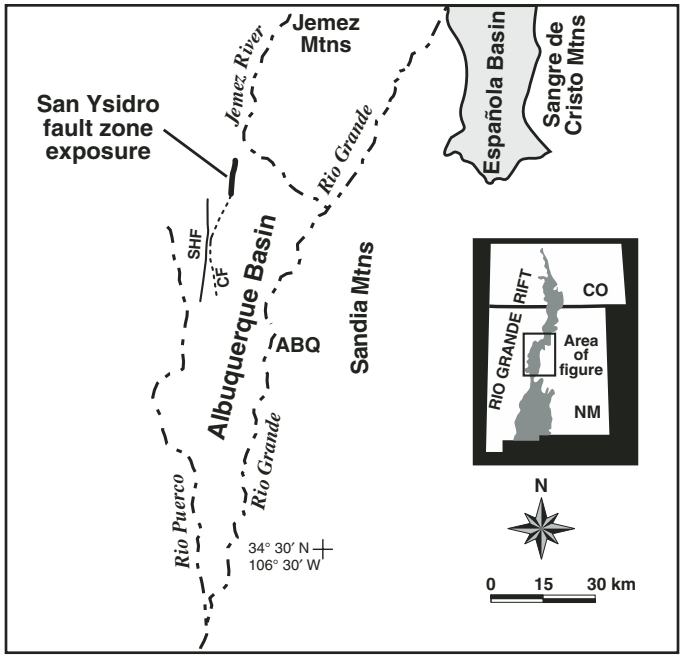

Figure 1. Location map of the exposure of the San Ysidro fault within the Albuquerque composite basin of the Rio Grande Rift. The locations of the Sand Hill (SHF) and Calabacillas (CF, dotted where concealed) faults are also shown. The city of Albuquerque is denoted by ABQ.

PREVIOUS WORK

The San Ysidro fault is one of several discontinuous faults aligned along strike in the northwestern corner of the Albuquerque Basin. These variably exposed faults define the complex western margin of the Rio Grande Rift south of the Valles caldera. Woodward and Reutschilling (1976) originally mapped the northernmost trace of the fault, which they called the San Ysidro fault. Kelley (1977) mapped the entire 48 km trace as the Jemez fault, whereas Kelson and Personius (1997) called it the Jemez–San Ysidro fault. Koning et al. (1998) and Connell et al. (1999), who mapped our focus area in detail, reverted to the original name of San Ysidro.

The San Ysidro fault zone is composed of distinctive structural, lithologic, and hydrogeologic components that have been described previously in faults formed in a variety of lithologies. These architectural components include: (1) a fault core where most of the strain has been accommodated (cf. Caine et al., 1996), which is surrounded by, and in sharp contact with, (2) mixed zones of entrained sedimentary beds, where a portion of the total strain may have been accommodated by particulate flow of clastic grains (cf. Heynekamp et al., 1999; Rawling and Goodwin, 2003, 2006) that are further enveloped by, (3) damage zones (cf. Chester and Logan, 1986) dominantly composed of deformation bands (cf. Aydin and Johnson, 1978; Shipton and Cowie, 2001). These components are surrounded by the protolith or undeformed host sediments (Fig. 2).

The San Ysidro fault is architecturally similar to previously studied faults in poorly lithified siliciclastic sediments (Minor and Hudson, 2006). These faults are distinct from faults that form in well-lithified sedimentary or crystalline rocks in that they do not have well-developed damage zones composed of open fractures (Rawling et al., 2001). Examples of faults similar to San Ysidro include the Sand Hill fault (Heynekamp et al., 1999; Rawling and Goodwin, 2006) and the Calabacillas fault (Doughty, 2003), both in the Albuquerque Basin (Fig. 1), and faults in the Roer Valley Rift system, the Netherlands (Bense et al., 2003).

The Sand Hill fault has a poorly developed, deformation-band–dominated damage zone, and a well-developed mixed zone (Heynekamp et al., 1999; Fig. 2). Rawling et al. (2001) showed that the presence of a mixed zone and the lack of open damage zone fractures can make these types of faults localized barriers (cf. Caine and Forster, 1999) that impede cross-fault

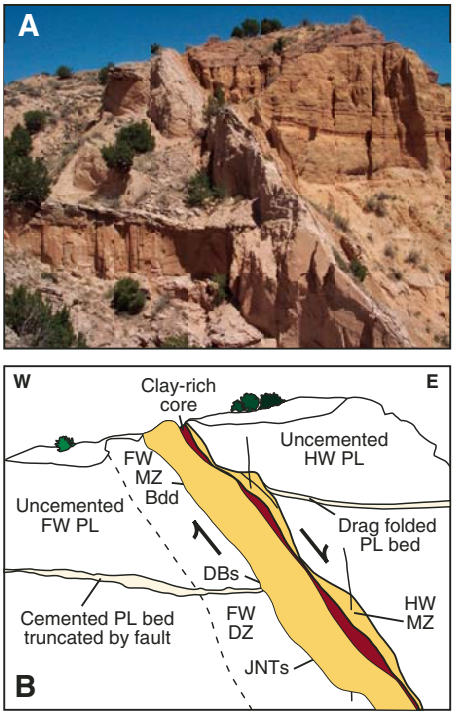

Figure 2. (A) Overview photograph of the San Ysidro fault zone looking north. (B) Schematic cross section showing the major boundaries of fault zone components as seen in the photograph. Note the fault-parallel orientation of attenuated beds in the footwall and hanging-wall mixed zones (highlighted in yellow). The dashed line is the approximate footwall damage zone–protolith contact. FW—footwall, HW—hanging wall, PL—protolith, DZ—damage zone, MZ—mixed zone, Bdd—bedding, DB—deformation band, JNT—joint.

fluid flow significantly more than faults with well-developed damage zones in lithified rocks. Rawling and Goodwin (2003, 2006) presented microstructural and macrostructural evidence that mixed zones formed by particulate flow and that transgranular fracturing and comminution were not necessary for strain accommodation.

The Calabacillas fault, exposed ~20 km to the south (Fig. 1), has less displacement than, but similar local stratigraphy to, the section of the San Ysidro fault studied here. The Calabacillas and San Ysidro faults are aligned, suggesting that the Calabacillas is a southerly continuation of the San Ysidro (Fig. 1; Personius et al., 1999; Connell, 2006). Doughty (2003) utilized heuristic models to conceptualize the development of clay smear in the core of the Calabacillas fault (cf. Weber et al., 1978; Lindsay et al., 1993; Egholm et al., 2008). In these models, clay smears develop through the mechanism of progressive formation of fault segments and releasing dip relays that ultimately link and establish the boundaries of the fault core (cf. Childs et al., 1996; Heynekamp et al., 1999). As the fault evolves, downward translation of the clay smears is facilitated by progressive strain localized within the fault core. Eventually, the smears may become separated from their sources. Subsequent thinning of the clay smears can locally result in higher permeability "holes" in the fault core (Heynekamp et al., 1999; Doughty, 2003).

In a regional survey of numerous fault zone exposures in poorly lithified sediments distributed throughout the northern Albuquerque Basin, Minor and Hudson (2006) observed architectural components similar to those that are characteristic of the San Ysidro, Calabacillas, and Sand Hill faults. A key observation from this work is the near ubiquity of laterally persistent clay-rich cores. Descriptive statistics of fault architectural measurements indicate considerable influence of the protolith lithology on fault zone architecture, component widths, component composition, and strain features (Minor and Hudson, 2006).

Little work has been done on the role of fluids in fault zone deformation in poorly lithified sediments. Although Rawling and Goodwin (2003) acknowledged the need for study of the role of fluids in the evolution of faults in poorly lithified sediments, it was beyond the scope of their research. Doughty (2003) did not discuss the role of fluids but proposed that clay plasticity—and, by inference, fluid content, composition, and source bed thickness—played a role in the development of the clay-rich smears in the fault core.

METHODS

Fault Zone Mapping and Characterization

Using the existing 1:24,000 scale geologic map by Koning et al. (1998) as a base, new mapping of the major San Ysidro fault zone components was completed at a scale of ~1:1000 in order to document the types, orientations, and positions of structures and their continuity along strike. Fault zone characterization was accomplished by map inspection and outcrop-scale identification and description of the structures, mineralogic variations, and general form and geometry of the fault zone. Detailed study of the fault core was completed along continuous horizontal and vertical cross-sectional exposures ranging from less than 1 m to over 8 m in length. Direct measurements of along-strike and downdip variations in width of each fault component were made using a tape measure. Estimates of fault displacement were made using dip separation of stratigraphic units from five cross sections at different positions along strike. Using a linear regression on dip separation versus position along strike from the cross sections, a regression equation was used to estimate dip separation anywhere along strike as well as to investigate relationships between fault component width and displacement.

Orientations of bedding, structural contacts, slip surfaces and lineations, deformation bands, calcite veins, and fault-related fold hinges were measured at numerous localities along the strike of the fault trace. Representative samples of each fault zone component were collected along seven traverses across the fault. Each sample was analyzed to determine: (1) microstructural and petrographic characteristics from thin section analyses, (2) mineralogy, (3) major-element and rare earth element composition, and (4) liquid and mercury injection permeametry.

Mineralogy and Geochemistry

Mineralogical and elemental analyses of faulted sediments were compared to protolith analogs to evaluate potential changes due to faulting. Due to large displacement, the fault core materials may not be directly related to the adjacent protolith. Representative samples from each fault component were collected along traverses across the fault for analytical comparison with exposed protolith sediments. Surface samples were excavated from tens of centimeters below outcrop faces to minimize inclusion of the most weathered material. Whole-sediment samples were analyzed for mineralogy by powder X-ray diffraction and for chemistry of major elements (using a four acid digestion with ±10% analytical error; see Briggs and Meier, 2002) and rare earth elements (REE; digested using a sodium peroxide sinter with ±5% analytical error; Meier and Slowik, 2002) using inductively coupled plasma–mass spectrometry (ICP-MS).

Powder X-ray diffraction (XRD) analyses of whole-sediment samples from the San Ysidro fault were completed at two different U.S. Geological Survey laboratories. Two methods were used to analyze the raw X-ray spectra, RockJock (Eberl, 2003) and SIROQUANT (Taylor, 1991), and each are briefly described next. All samples were crushed to a 150 µm powder, micronized in a mill to an average grain size of ~5 µm, and then side loaded into holders to ensure random mineral orientation. The samples were X-rayed with Cu-K_α radiation from 5° to 65° two theta (Boulder Lab for RockJock) or 4° to 90° two-theta (Denver Lab for SIROQUANT) using 0.02° two-theta steps and a scan time of 2 s per step.

Figure 3. Geologic map of the San Ysidro fault showing the local stratigraphic section and structural data collected along the full length of the exposed fault zone plotted on lower-hemisphere equal-area projections. The mapped geology and stratigraphy are modified from Koning et al. (1998) and Connell et al. (1999). Quat—Quaternary, Pleisto—Pleistocene, Plio—Pliocene, Fm—Formation. The topographic base is from U.S. Geological Survey digital elevation model data, Cerro Conejo, New Mexico, 7.5′ quadrangle. (A) Equal-area projection showing the great circles and tangent lineations for slip surfaces in the fault core and mixed zone. Arrows accompanying each tangent lineation indicate the movement direction of the footwall. The thick, black great circle and corresponding black tangent lineation with gray outline correspond to the mean slip surface and lineation. (B) Comparison of poles to bedding within (black) and outside (gray) the fault zone. (C) Comparison of poles to deformation bands (medium gray diamonds), joints (dark gray triangles), and veins (light gray circles). In B and C, the mean vector orientations for each type of structure are shown as corresponding, enlarged symbols.

RockJock Analyses

The mineral phases are identified, and then a standardless RockJock analysis (i.e., no added internal standard) was used to convert the XRD intensity data into mineral weight percents using the RockJock computer program (Eberl, 2003). Integrated XRD intensities were determined by whole pattern fitting (Smith et al., 1987) using a library of XRD patterns of pure minerals. Several patterns of individual minerals from the library were scaled simultaneously and summed together to create a calculated pattern that was compared to the measured sample pattern. The scaling factors were adjusted automatically until the degree of fit between the measured and calculated patterns was minimized. The error in the analyses was approximately ±3 wt% (one standard deviation) at 50 wt% of a mineral (Eberl, 2003). Each sample underwent at least two RockJock analyses.

SIROQUANT Analyses

An internal standard of Al_2O_3 (corundum) with an average grain size of 1 μm was added to each sample (10% by weight) to help in the quantification of amorphous material as well as crystalline phases. The subsequent quantitative analyses were carried out using the SIROQUANT Rietveld full-profile phase quantification program (Taylor, 1991). Mineral X-ray patterns were calculated from their crystallographic parameters (Rietveld), summed together, and then compared to the measured pattern. However, clays and solid solution minerals could not be fully described mathematically to allow a calculation of their XRD patterns. Instead, scans of pure minerals (full profile) available from the SIROQUANT database were scaled and summed together with the calculated mineral patterns and fit to the measured X-ray patterns using a least-squares regression. The X-ray results have relative standard deviation values that range from ±3%–5% for phases over 30% by weight, ±10%–15% for phases from 10% up to 30% by weight, ±20%–25% for phases from 3% to 10% by weight, to ±30%–40% for phases below 3% by weight.

Fault Zone Component Permeability

The permeability of each fault zone component was measured using core-plug liquid permeametry and, for fault core clay samples, mercury injection capillary entry pressure permeametry. Detailed methods, data, and results for these measurements can be found in the GSA Data Repository (Fig. DR3; Table DR7).[1]

LOCAL GEOLOGY OF THE FAULT

On the basis of existing geological maps, topographic lineaments, and high-resolution aeromagnetic data, the San Ysidro fault has an approximate total strike length of 48 km (Kelley, 1977; Cather et al., 1997; Kelson and Personius, 1997; Sweeney et al., 2002). The exceptional 10-km-long exposure of the San Ysidro fault that is the focus of this paper is located along the central part of the fault trace (Figs. 1 and 3). Based on our mapping and previous mapping by Koning et al. (1998), we estimate that ~67% of the fault core and adjacent mixed zones are well exposed along a composite strike length of 3.4 km within the 10-km-long exposure mappable as a largely continuous, single structure (Fig. 3).

Most faults in the basin are normal faults and have 10–30 km trace lengths. Little is known about the magnitude of displacement along them, whether and how these faults are segmented and linked, and whether they ruptured Earth's surface during their evolution. The San Ysidro fault strikes north and dips an average of 66° to the east (Fig. 3; Fig. DR1; Table DR1 [see footnote 1]). Slip lineation data from numerous localities along the fault indicate predominantly dip-slip displacement of subhorizontal beds (Fig. 3). Dip separation along the strike of the fault shows a nonconstant gradient from 440 m in the south to 680 m in the north (Fig. DR2; Table DR [see footnote 1]).

Beds that have been entrained into the fault zone have dips up to 82° to the east to northeast (Fig. 3). Along strike, variation in the rake of slickenlines indicates variable oblique slip that appears to be controlled by the geometry of the fault core, particularly where it curves or jogs, such as adjacent to the "Horsetail" feature at the northern end of the fault exposure (Fig. 3; see GSA Data Repository for detailed data and discussion of the shape of the fault [see footnote 1]). The Horsetail is an area of broadly distributed, subparallel small-displacement faults in the San Ysidro hanging wall at the point of maximum curvature of a major left step (Fig. 3). At this point, the slip lineations on the western, fault core bounding slip surface of the main fault abruptly change from dip slip to dextral-oblique slip. Farther south, several clastic dikes are observed in the footwall.

SAN YSIDRO FAULT ZONE ARCHITECTURE

Damage Zone

The damage zone is characterized primarily by deformation band faults (cf. Aydin and Johnson, 1978) generally exhibiting <1 cm of separation. They range in intensity from ~0.1 to 1 fault per meter. Individual faults range in character from less than 1-mm-wide individual deformation bands to groups of coalesced deformation bands several centimeters thick. Deformation band faults generally strike north and have dips that are synthetic or antithetic with respect to the main trace of the fault zone (Fig. 3). In the Horsetail region, deformation bands maintain synthetic-antithetic orientations but appear to change strike similar to the main trace of the fault zone (Fig. 3). Less common structures are small-displacement (typically ≥10 cm but ≤1 m), synthetic and antithetic faults (Fig. 3). Other structures include joints that are also locally present in the undeformed protolith and cut all other architectural components (Figs. 2

[1]GSA Data Repository item 2009132, provides supplementary information on fault displacement, age, slip rate, shape, orientation, kinematics, fault component width distributions and relationships to displacement, and permeametry, is available at http://www.geosociety.org/pubs/ft2009.htm or by request to editing@geosociety.org.

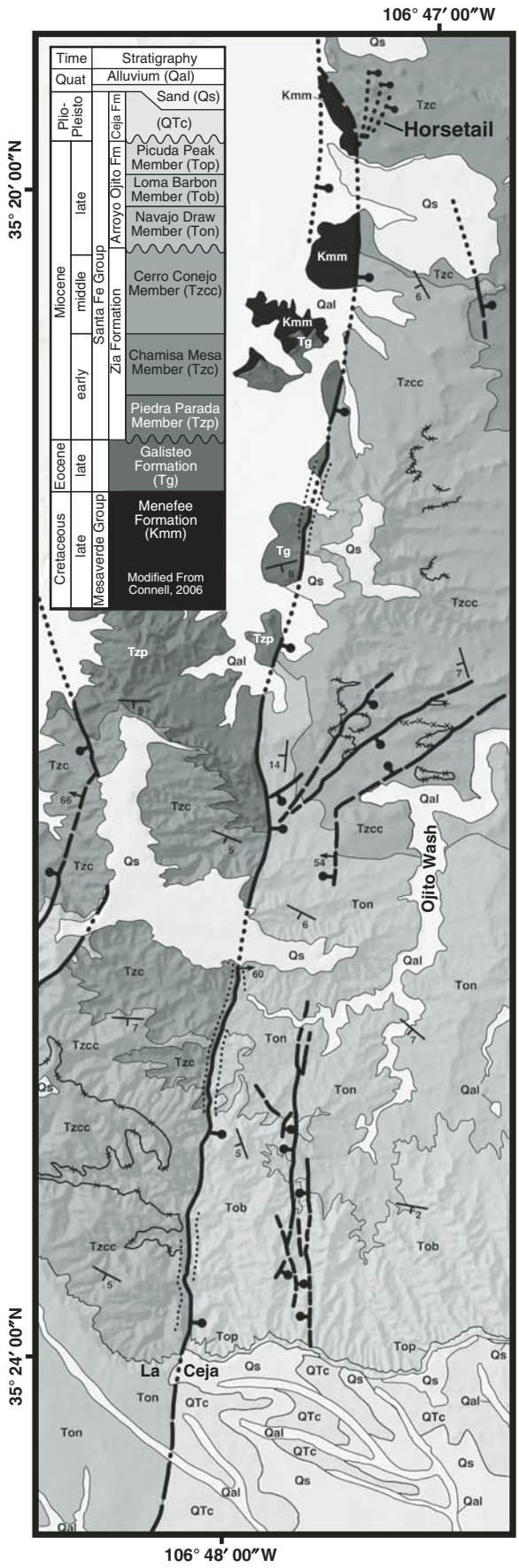

EXPLANATION

400 0 400 800 meters

54 — San Ysidro fault: Solid where clay-rich core is exposed,dashed where inferred from partial exposures and aeromagnetic data, dotted where concealed. Ball and bar on down dropped side. Arrow shows dip and dip direction.

Sedimentary contact

6 — Strike and dip of beds.

Damage zone boundary (inclusive of mixed zone): Where partially exposed and inferred.

Ash beds geochemically correlated with ca. 11 Ma. ashes from Idaho.

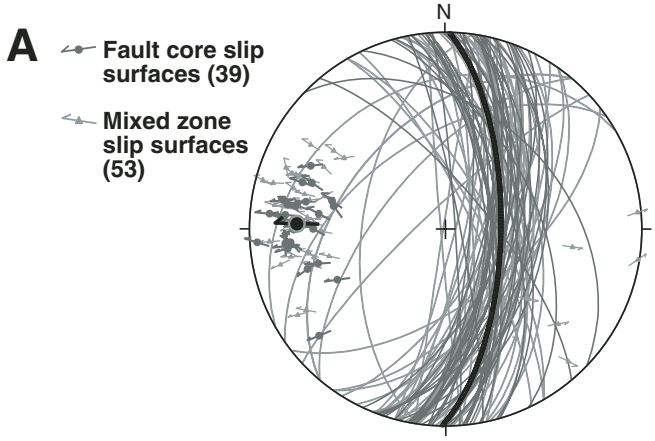

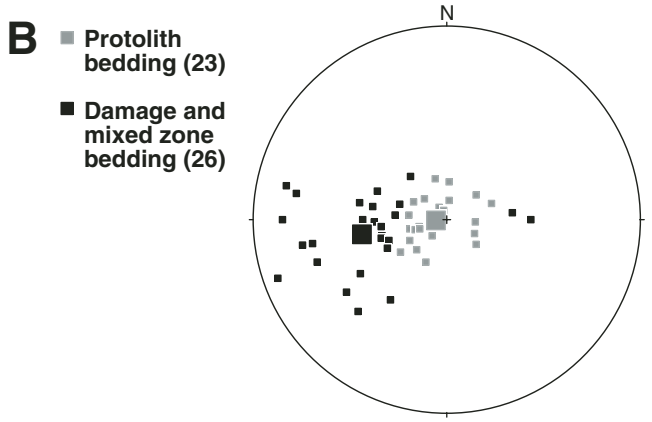

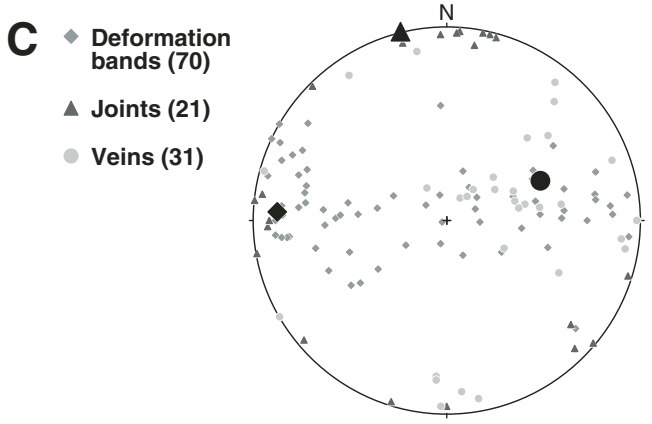

and 3). Joints are near vertical; the most dominant set strikes approximately east-west (Fig. 3). The nature of the footwall and hanging-wall damage zone contacts with the mixed zone is variable. The contacts are commonly irregularly shaped zones of deformation bands and (or) slip surfaces that separate subhorizontal beds from rotated beds. Along some traverses, damage zone width is asymmetric, with the hanging-wall damage zone locally absent.

Mixed Zone

Between the damage zone and fault core, there is a zone of entrained beds similar in structural and physical character to that observed by Heynekamp et al. (1999) and Rawling and Goodwin (2003, 2006) along the Sand Hill fault, and those observed by Minor and Hudson (2006) along most faults exposed in the northern Albuquerque Basin. Materials entrained into what Heynekamp et al. (1999) called a "mixed zone" range from largely intact but friable sedimentary beds up to 1 m in thickness and 4 m in length, to friable mixtures of silt, sand, and gravel that have no remnants of original sedimentary layering. Relatively intact entrained beds have been rotated into orientations subparallel to the fault core (Fig. 3). Where present, variably mixed materials are generally confined to small volumes between intact entrained beds but also randomly cut these beds in irregularly shaped bodies.

Entrained beds rotated parallel to the fault core have been cemented by sparry calcite at numerous localities along the strike of the fault. Field observations qualitatively indicate that cement in the fault zone appears to be most abundant in the footwall mixed zone. Calcite cementation also has preserved sand beds that have been folded and attenuated in the mixed zone at several localities (Figs. 4 and 5). Additionally, deformation bands and sparry calcite veins cut the cemented, entrained beds. Sparry calcite veins have a somewhat dispersed distribution of orientations, including a diffuse NNW-striking and moderately to steeply west-dipping mean set and a subvertical east-striking set (Fig. 3). Our thin section analysis of calcite-cemented, mixed zone samples shows little evidence of fault-related intragranular or intergranular fracturing or cataclasis except where cut by deformation bands.

Figure 4. (A) Calcite-cemented bed at the footwall damage zone–mixed zone contact in the southern segment of the San Ysidro fault zone preserves a "drag" fold. (B) A similarly rotated, attenuated, sheared, and cemented sand bed. The hammer is parallel to the dip of unrotated subhorizontal bedding, and the field notebook is parallel to the dip of the entrained and rotated portion of the bed. Note the near vertical slickenlines on the slip surface that cut the bed. Field notebook is 12 cm wide.

Mixed Zone–Fault Core Contact

The San Ysidro mixed zone–fault core boundary is everywhere sharp and is commonly bounded by well-defined slip surfaces (Fig. 5). Unlike fault core–bounding slip surfaces in lithified rocks, San Ysidro bounding slip surfaces typically are unpolished and show no evidence of silicification. In some cases, these surfaces are parallel to fault-entrained and attenuated bedding surfaces that host ridges and grooves indicating normal dip slip. Local sparry calcite cementation at the contact has preserved a variety of slip lineations, slip surfaces, and other structures (Fig. 5). Many of the cemented slip surfaces differ from slip surfaces commonly observed in faults in well-lithified rock in that they exhibit slip-parallel linear, curviplanar, and convoluted features that curl over in wave-like forms. Many of

these features are rather large; dimensions can be several tens of centimeters long and up to several centimeters wide and deep. On some slip surfaces, there are sole-mark or flame-like features that are similar to fluid escape structures found in sediments that have undergone soft-sediment deformation (cf. Lowe, 1975; Petit and Laville, 1987). However, these are linear features that are generally well organized and aligned parallel to other dip-slip kinematic indicators.

In a few locations, we observed vertically elongate, sparry calcite-cemented concretions similar to those described by Mozley and Goodwin (1995). These are rather large, column-like features that are tens of centimeters long and a few centimeters in diameter with no visible internal bedding. Where slip surfaces are uncemented, the convolute features similar to the cemented structures described previously are observed but are not as well defined. Sparry calcite veins everywhere cut the slip surfaces and various other fault-related structures (Fig. 5).

Fault Core

Where exposed, the fault core ranges from clay-sized material that is dominated by clay minerals to a mixture of grain sizes including clay, silt, sand, and pebbles. In some localities, the core is internally segregated and characterized by fault-parallel clay-rich units or bands of distinctive color (Fig. 6). In many of these clays, there is no evidence of bedding and (or) laminations. The clay bands are distinguished by their green-gray and, more commonly, red-brown color, which contrasts strikingly with the generally beige siliciclastic host sediments. Typically, curviplanar margins of the fault core clay units completely conform to any surface or feature with which they are in contact or juxtaposed (Fig. 6).

Other features of the core include incised and noncylindrical, convoluted surfaces with curvilinear ridges and furrows of clays generally aligned in the direction of slip. In some examples, the crests of the convolutions are folded back upon themselves in an irregular manner (Fig. 6). Some of these features are similar to those present in the sands of the mixed zone but are commonly smoother, more irregularly shaped, and have generally smaller dimensions. Slip surfaces in the San Ysidro clay core have some similarities to "ridge-in-groove" slickenlines of Means (1987), but they are more irregular, quite large, and deeply incised, and they do not necessarily define a highly organized foliation. Features within the clay core, such as irregular chunks of sediment, dismembered clay beds, macroscopic lithic clasts, and other

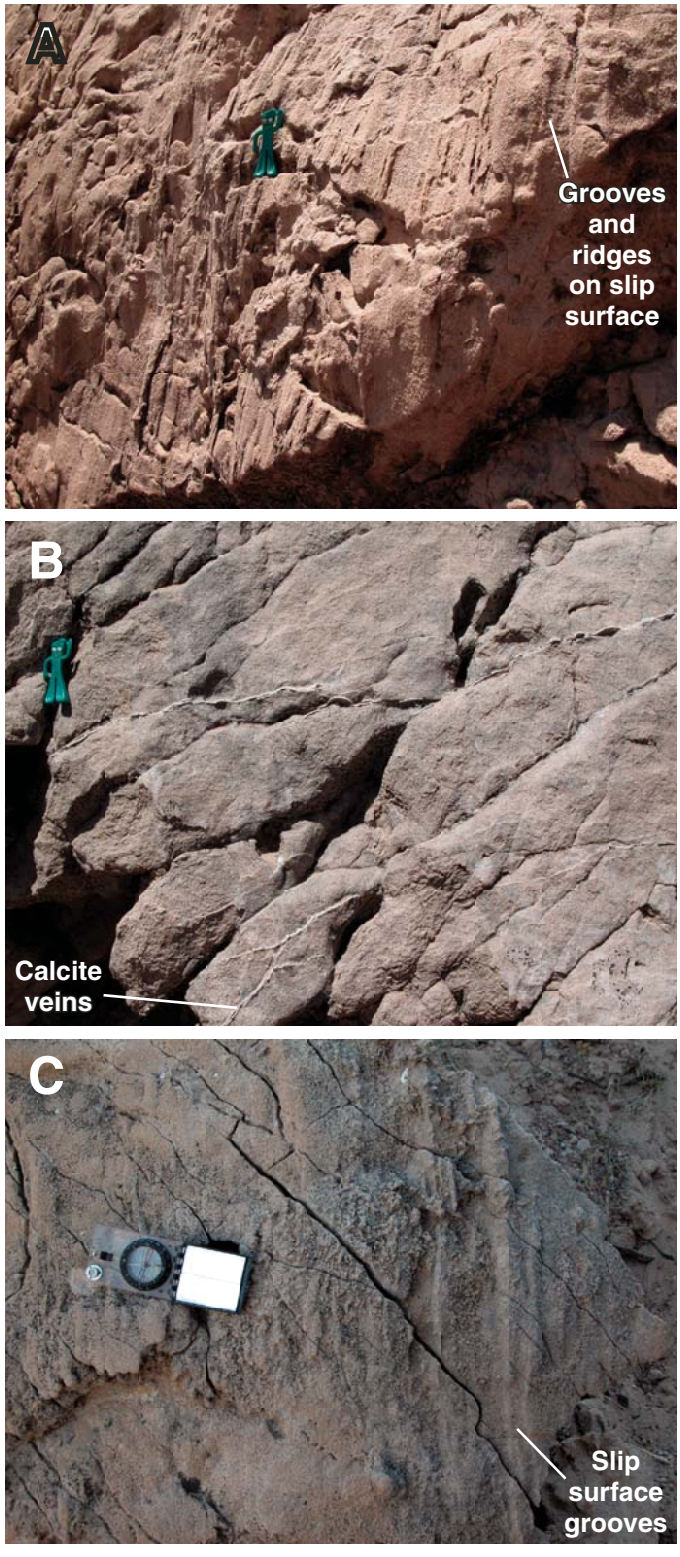

Figure 5. (A) Photograph of a large, unpolished slip surface on an entrained and calcite-cemented sand bed at the footwall mixed zone–core contact. The grooves and ridges are on a bedding plane subparallel to the outcrop surface and parallel to the slip direction. Gumby is 8 cm tall. (B) Detail of calcite veins that cut the structures in A in the lowermost left corner. Gumby is 8 cm tall. (C) Detail of a slip surface showing grooves plunging downdip, a knob in the central lower portion of the photograph, and slip-parallel convolutions. Note the open, crosscutting diagonal fractures. Compass is 6 cm long.

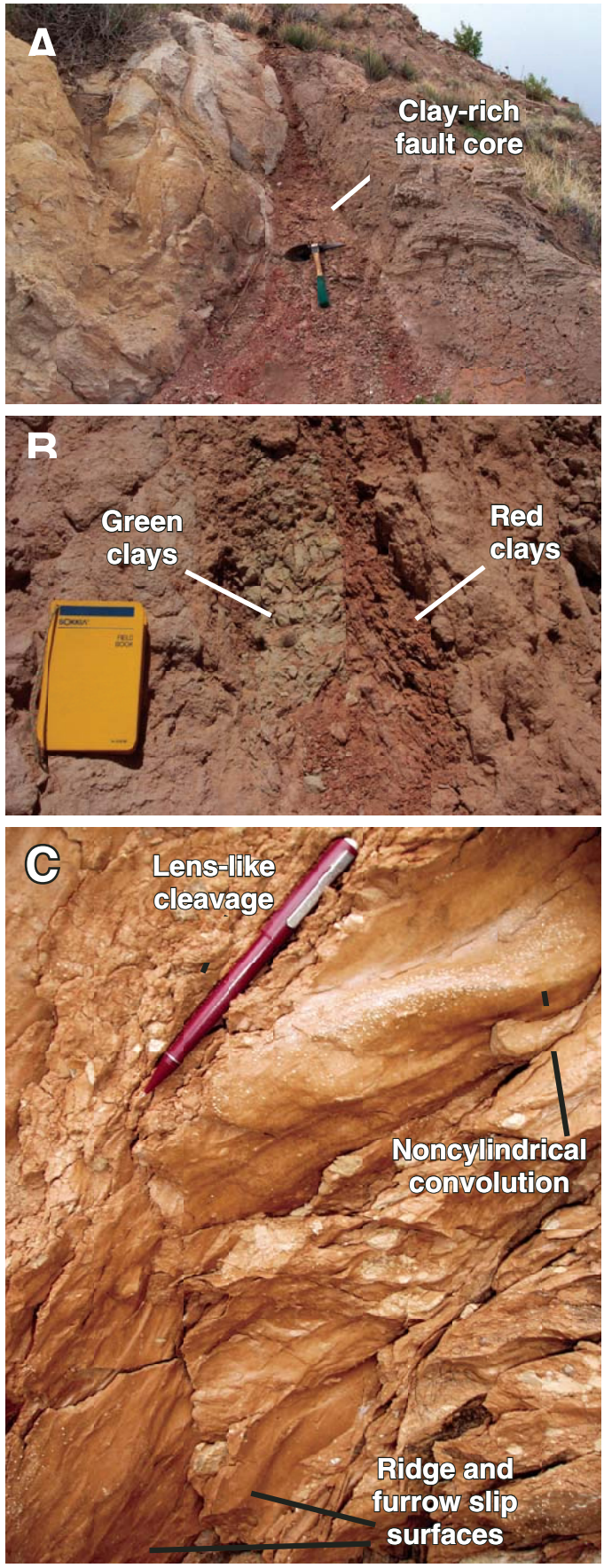

Figure 6. (A) Photograph looking north at the clay-rich fault core where it abruptly thins from >1 m to 6 cm in width. The core in this exposure is composed of nearly pure, red-brown clay, and it shows foliation subparallel to the nominal plane of the fault. Pick handle is 0.3 m long. (B) View of clay core with entrained and juxtaposed red-brown and green clay at an exposure ~3 km south of the exposure shown in A. Field notebook is 12 cm wide. (C) Close-up view of an exceptional example of a large noncylindrical convolution, internal ridge and furrow-like slip surfaces with small protruding asperities, cross-cutting lens-like cleavage, and lithic clasts and chunks of entrained sands in a brown, clay-rich fault core from the Santa Clara fault zone in the Española Basin northeast of the San Ysidro fault. Similar features observed in the San Ysidro fault core are typically quite small, as they are in clay-rich fault cores throughout the basins of the middle Rio Grande Rift. The pencil is 14 cm long and is lying in the nominal plane of the cleavage.

grains strung out along curviplanar trains parallel to the fault, are completely enveloped by the clays. All of these resemble features observed in other clay-rich fault cores in poorly lithified sediments throughout the middle Rio Grande Rift (e.g., Minor and Hudson, 2006).

Small, 1-cm-thick sand injections locally cut entrained beds of the mixed zone, refract irregularly into the adjacent clay core, and pass out the opposite side. Moderately well-developed, but irregular lens-like cleavage hosting minor, polished slip surfaces is present in many clay-core exposures, particularly where the clay content is high (Fig. 6). Where this cleavage is well developed, slip surfaces commonly not only cut the clay units, but also cut internal clasts, ridges, and furrows. In a few exposures, small faults with centimeters of displacement and no calcite cementation cut the clay-core materials, convolute structures, and cleavage developed within it. Only rarely does the fault core show sand-on-sand juxtaposition or brecciation of all of the core materials.

Fault Zone Architectural Widths and Relations to Displacement

As mentioned already, a damage zone is not present everywhere along the San Ysidro fault. Where present, damage zone widths (i.e., thickness between bounding contacts) were estimated by measuring from the mixed zone edge to where there is a subjective macroscopic decrease in deformation band intensity relative to the adjacent protolith. Hanging-wall and footwall damage zone widths range from 2.4 m to 59.8 m and average 20.9 m. The mixed zone ranges in width from 0 to 7.5 m in the footwall

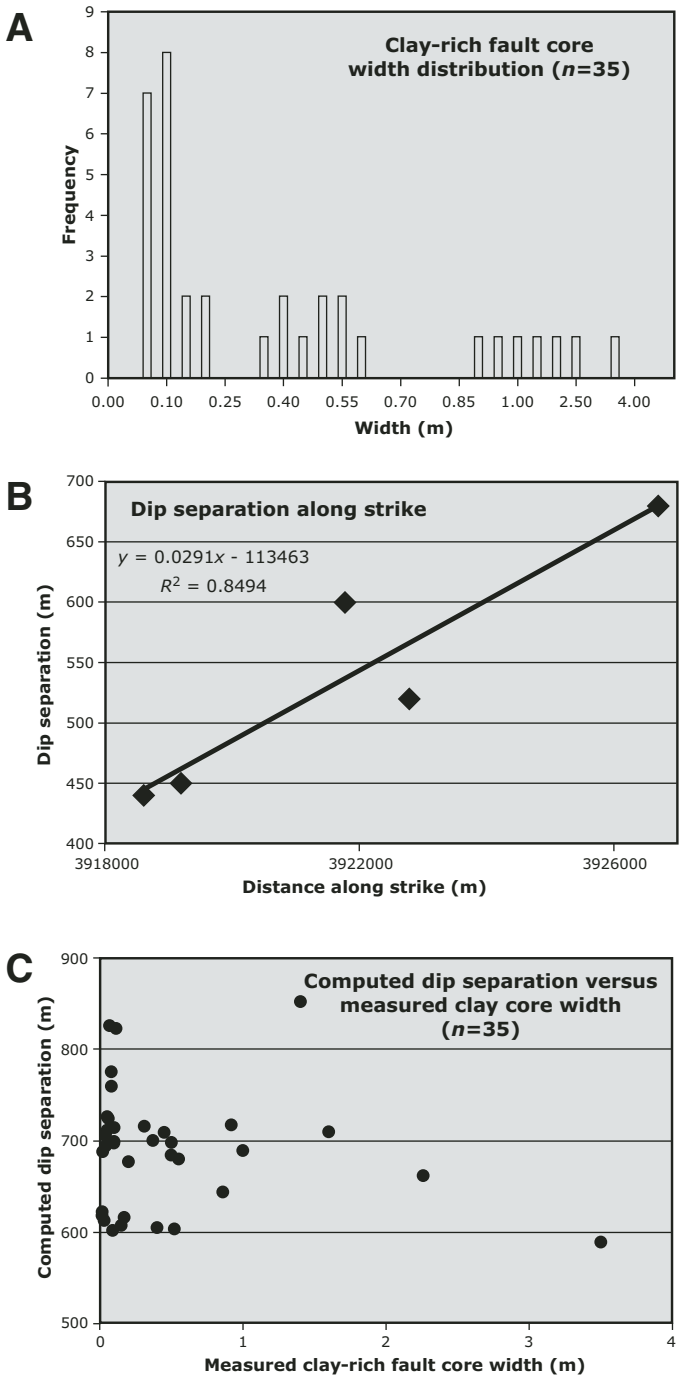

Figure 7. (A) Histogram of clay-rich fault core width measurements at 35 localities along the strike of the San Ysidro fault. (B) Plot of dip separation estimates derived from cross sections across the San Ysidro fault (see Fig. DR2 [see text footnote 1]) versus distance along strike, showing linear regression results. R^2 = regression correlation coefficient. (C) Plot of computed dip separation derived from the regression equation in B versus fault core width along strike of the San Ysidro fault.

and from 0 to 4.5 m in the hanging wall. Other than at a few rare exposures where there is sand-on-sand juxtaposition and the fault core is exceptionally thin, the core ranges in width from 0.02 m to 3.50 m, with a median of 0.17 m and a mode of 0.10 m (Figs. 6 and 7; Tables DR2 and DR3 [see footnote 1]).

When all fault architectural component widths are added together (cf. Caine et al., 1996), the total cross-sectional fault zone widths range from 9 to 99.6 m, with a median of 45.4 m, for seven traverses across the fault where each component was measurable (Table DR2 [see footnote 1]). The sample size is small, and frequency histograms of total fault width, or any other fault component width in the footwall or hanging wall, show no functional distribution except for a possible log-normal frequency relationship of fault core widths (Fig. 7; Table DR2 [see footnote 1]).

Figure 7 also includes a scatter plot of computed dip separation versus measured fault core width using the equation derived for dip separation along strike. A linear regression of the resulting paired values of separation versus width results in a poor correlation ($R^2 = 0.009$), consistent with the field observation that fault core width is not well correlated with displacement in the San Ysidro fault (Fig. 7; cf. Shipton et al., 2002). Field observations also show that there is no correlation with width for any of the other fault components with either displacement or position along strike. Minor and Hudson (2006) observed a similar lack of correlation for the faults they studied elsewhere in the northern Albuquerque Basin.

MINERALOGY AND ELEMENTAL GEOCHEMISTRY

Sample mineralogy and major and rare earth elemental geochemistry results are plotted in Figures 8, 9, and 10 (from data provided in Tables DR4, DR5, and DR6, respectively [see footnote 1]). The data are plotted for each architectural component where it could be sampled along seven traverses across the fault. The number of samples for any component is not large, ranging from 2 to 8 in number, and therefore samples do not represent the full potential range in variability. It is also important to reiterate that the sample sets only reflect the current structural levels and juxtapositions along the fault. Thus, they do not provide a direct comparison between fault core and protolith source bed compositions due to the large displacements across the fault.

Protolith and mixed zone samples are grouped according to the degree of calcite cementation of dominantly siliciclastic sand (Fig. 8). In general, the highest concentrations of calcite are found in the footwall mixed zone. Two clastic dike samples are generally quartz-rich and clay-poor, and one is calcite cemented.

The fault core is predominantly composed of clay. However, variable mixtures of clay, silt, sand, and lithic clasts that are mineralogically similar to the protolith siliciclastic sediments also have been identified (Fig. 8). Clay mineral data are grouped together as total clay and as

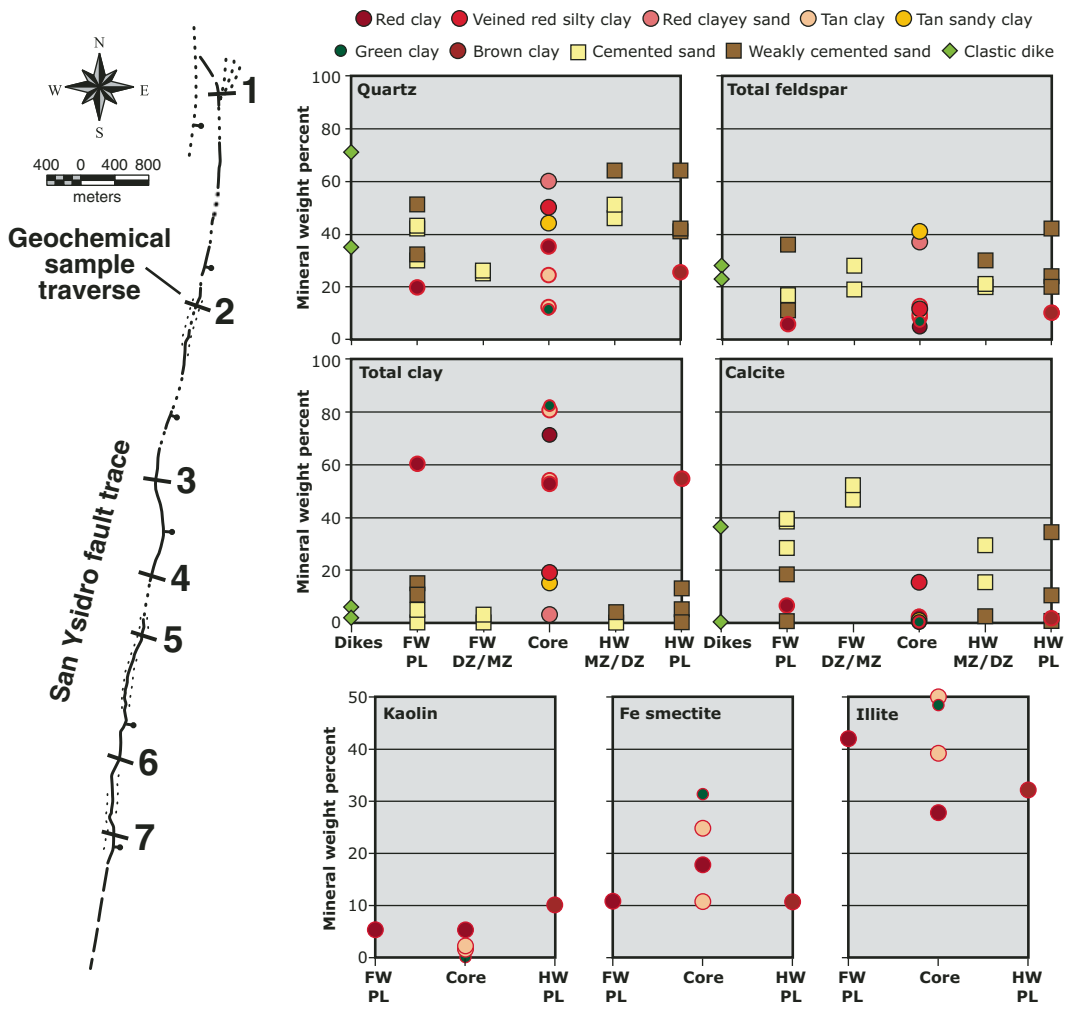

Figure 8. Plots of X-ray diffraction (XRD) mineralogy for common rock-forming minerals found in the San Ysidro fault using both RockJock (symbols outlined in red) and SIROQUANT methods. The plots are organized as mineral weight percent versus fault zone component (clastic dikes; footwall and hanging-wall protolith, damage, and mixed zones; and fault core). The different symbols plotted indicate bulk lithology and degree of calcite cementation, as defined in the legend at the top. The lower three plots show detailed clay mineralogy for the fault components indicated (RockJock analyses only). The numbered locations of the sample traverses relative to the fault trace are shown at left. Abbreviations: FW—footwall, HW—hanging wall, PL—protolith, MZ—mixed zone, DZ—damage zone.

individual clay minerals for a small subset of the samples obtained from the most pure clay cores and the two protolith clays that were analyzed (Fig. 8; Table DR4). Total clay concentrations of the protolith samples fall within the variability of the fault core samples. The fault core sample with the highest total clay concentration has 43% more total clay than the mean value of the two protolith samples. The dominant clay minerals include kaolinite, ferruginous smectite, and illite. Relative to the protolith, the core has the following: (1) generally less kaolinite, (2) nearly three times as much ferruginous smectite, and (3) variable illite concentrations that are a maximum of 35% greater than the mean protolith values.

The major rock-forming elements of fault component samples are shown in box plots in Figure 9 (Table DR5 [see footnote 1]). The samples are grouped as clay protolith; clastic dikes; weakly cemented versus cemented footwall and hanging-wall protolith and mixed zone sediments; and clay-rich versus clay-sand mixtures from the fault core. The absolute differences in mean concentrations between each group are generally small in magnitude, within several percent, and most fall within the range of variability of the data for each (Fig. 9). Calcium is an exception; the absolute difference for calcium is higher by up to 15% in the footwall and hanging-wall mixed zone sediments relative to any other fault component due to calcite cementation (Fig. 9). In addition, the relative percent difference of mean elemental concentrations beyond analytical error (±10%) between the clay protolith and some of the entrained clay-rich and clay-sand mixtures in the fault core is substantial. Relative to the two protolith clay beds, the clay-rich fault core samples have 30%–54% higher mean concentrations of iron, magnesium, and potassium (Table DR 5 [see footnote 1]). No substantial elemental decreases are observed between the protolith clays and clay-rich fault core samples. However, clay protolith compared with fault core clay-sand mixtures shows relative percent decreases of 22%–52% in all elements except potassium. In fact, the fault core clay-sand mixtures tend to fall between the clay and sand protoliths for most elements (Fig. 9). Although box plots aggregate all sample data from individual traverses across the fault zone, the variations among the mean values from different traverses within any single fault component, and along the strike of the fault, show similar patterns to the individual traverses.

Chondrite-normalized (cf. Anders and Ebihara, 1982) rare earth element (REE) patterns are shown in Figure 10 and Table DR6 (see footnote 1), where the data are grouped in the same manner as they were for the XRD data. REE patterns of the clays and clay-rich sediments from the protolith and mixed zone are essentially identical to those of the clays in the fault core, with a distinct negative europium anomaly. REE patterns from the hanging-wall clay-rich protoliths are nearly identical to those of the footwall. The REE patterns also appear to reflect clay content, since pure clay samples

tend to form groups, as do the progressively more sand-rich samples.

Calcite-cemented sediments, sediments with deformation bands, and crosscutting sparry calcite veins have distinct REE patterns (Fig. 10). Calcite-cemented sediments from all fault components, in both the footwall and the hanging wall, show generally lower values for light REEs, negative cerium anomalies, and relatively similar or higher values for heavy REEs than the weakly cemented to uncemented sediments. The sparry calcite cement is also distinct from a sparry calcite vein sample because the vein has the overall lowest concentration of light REEs and the most negative cerium anomaly. Clastic dikes show REE patterns essentially the same as the host siliciclastic sediments except that the more cemented of the two dikes sampled has lower light REE values, consistent with the more cemented host sediments.

ESTIMATES OF FAULT ZONE COMPONENT PERMEABILITY

To evaluate the permeability contrasts in components of the San Ysidro fault zone, representative samples were collected along seven traverses across the fault (Fig. 8). The minimum permeability measured, 3.0×10^{-20} m^2, was from the clay-rich fault core. The maximum, 6.8×10^{-12} m^2, was from uncemented, coarse sand from the footwall protolith (Fig. DR3; Table DR7 [see footnote 1]). This ~6.5 orders of magnitude permeability contrast between the clay core and protolith is representative of the fault zone as a whole and is consistent with previous work on the Sand Hill fault by Rawling et al. (2001). Because unoriented samples of the clay-rich fault core were used for these analyses, permeability anisotropy within the fault core could not be evaluated. However, five cores were drilled from oriented, carbonate-cemented sand samples collected from the mixed zone to evaluate permeability anisotropy in beds entrained into the fault. Most of these directional samples were nearly isotropic; the maximum anisotropy measured was about one order of magnitude; and the maximum permeability direction was parallel to bedding and the nominal plane of the fault into which it was entrained (Table DR7 [see footnote 1]).

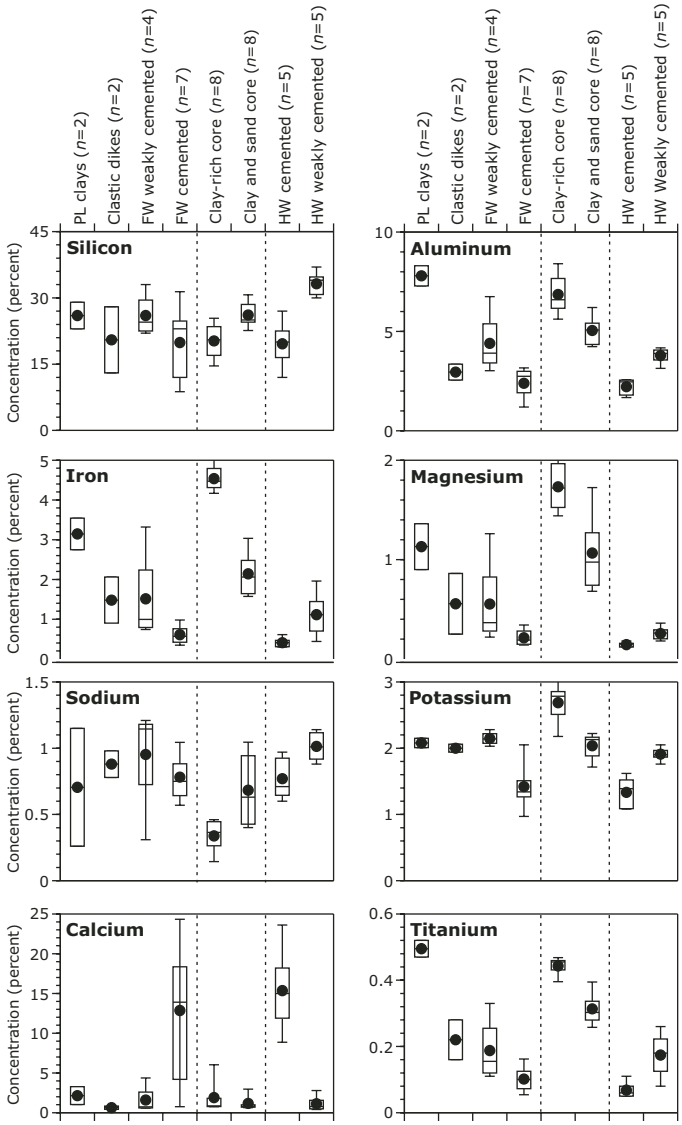

Figure 9. Box plots showing the elemental concentrations (in percent) of eight common rock-forming elements for all samples. Groupings include protolith clays, clastic dikes, footwall and hanging-wall damage and mixed zone samples grouped together but differentiated by degree of calcite cementation, and two groupings of samples from the fault core, clay-rich and clay sand mixtures. The fault core data are separated by dashed lines. Each box shows the concentrations of the 75th percentile (top box edge), the median (black dot), mean (intermediate line), and 25th percentile (bottom box edge) for each component. The top and bottom whiskers show the concentrations of the 10th and 90th percentiles, respectively. Abbreviations: FW—footwall, HW—hanging wall, PL—protolith, *n*—number of samples.

DISCUSSION

Field observations indicate that protolith sediment was entrained into the San Ysidro fault zone. Cemented sand beds record folding where beds were rotated at the margins of the mixed zones (Fig. 4). Beds preserved in the mixed zones dip steeply and have been thinned to varying degrees (Fig. 11). Thinning appears to have occurred without the development of discrete structures, since there is a notable absence of fractures in the mixed zones from the mesoscopic to the microscopic scale. The only exceptions are sparry calcite veins and few deformation bands that postdate mixed zone cementation.

The steeply dipping fault core is a single, nearly continuous structure, pervasively clay-rich, and in sharp contact with the sand-rich mixed zone. Within the clay-rich core, there is segregation of distinct, differently colored thin clay bands, many without evidence of bedding.

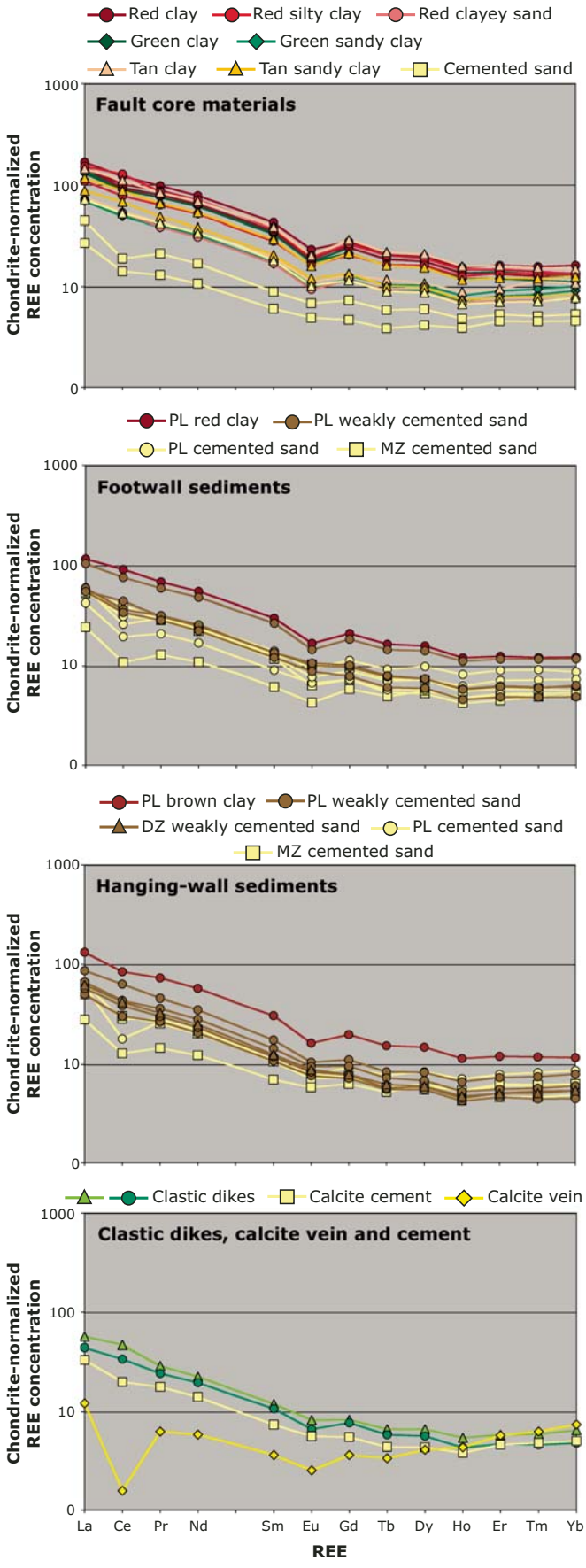

Figure 10. Plots of chondrite-normalized rare earth element (REE) data organized by fault core and footwall and hanging-wall sediment samples. The various line and point symbols and colors indicate bulk lithology and degree of calcite cementation, as defined in the legend at the top. Abbreviations: PL—protolith, MZ—mixed zone, DZ—damage zone.

Within these clay bands, there locally are trains of siliciclastic grains strung out in parallelism with the fault. Nonclay grains and grain aggregates in the core are always completely enveloped by clays, as are the convolute contacts with the siliciclastic mixed zone. Fault-parallel cleavage within the clay-rich core cuts but does not displace various internal features such as bedding. This suggests that cleavage was secondary to the initial entrainment of material in the core. This cleavage also was subsequently cut by small faults.

Observations from the mixed zone and clay core—particularly the evidence of extreme thinning of sand beds and likely of clay bands without primary fracturing—support an interpretation of initial deformation through distributed particulate flow in these poorly lithified sediments. Stratigraphic considerations suggest that deformation occurred at depths ranging from the near surface to no more than ~1 km. The degree of groundwater saturation, or depth relative to the paleo–water table, cannot be similarly constrained, but it must be inferred from circumstantial evidence. Clastic dikes and sand injections that cut the fault core provide evidence of complete saturation of the sand source, which is unlikely to be far from the injection sites. Mixed zones were cemented subsequent to at least part of the deformation history. Cements are coarse crystalline calcite, consistent with phreatic cementation. These pieces of evidence support, but do not conclusively prove, an interpretation of saturation during deformation.

More provocative evidence supporting deformation in a saturated state is provided by outcrop-scale structures. Structures similar to the grooved and convolute margins we have observed at the contacts between fault-entrained lithologic layers were previously interpreted by Petit and Laville (1987) as recording deformation in a water-saturated state. However, Petit and Laville were also unable to prove saturation at the time of faulting. Significantly, Clausen and Gabrielsen (2002) recently conducted a series of deformation experiments on water-saturated clays and clay-sand mixtures using a ring-shear apparatus. In these room temperature laboratory shear experiments, the role of

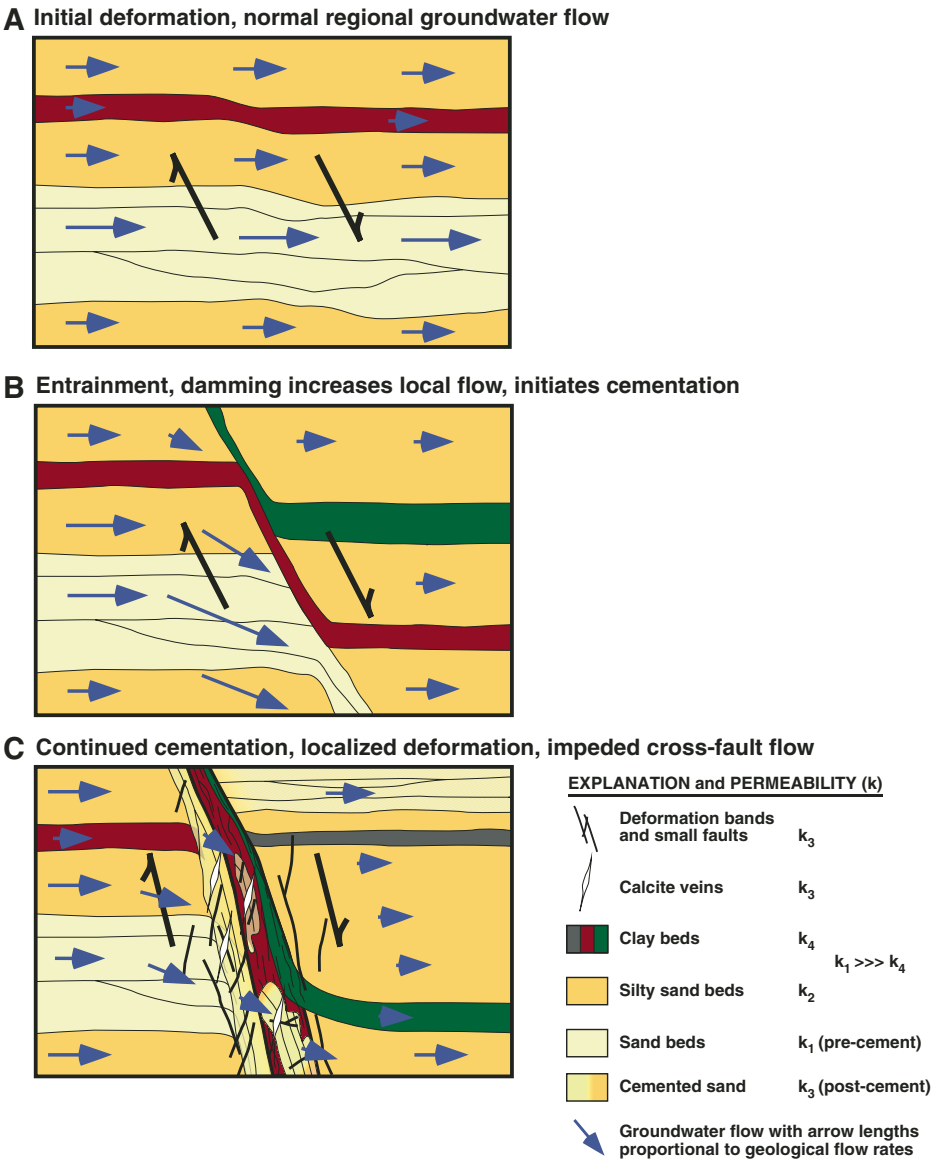

Figure 11. Schematic diagrams of three possible stages in the inferred conceptual model for the formation and evolution of the San Ysidro fault. Black arrows indicate relative motions of the footwall and hanging wall, and blue arrows indicate the direction and relative magnitude of groundwater flow controlled by the evolving permeability structure of the fault. (A) Initial deformation inferred to be at low temperature and pressure in the paleo–saturated zone with essentially unperturbed regional, lateral groundwater flow controlled by the bulk permeability (*k*) of each stratigraphic unit. (B) During growth of the fault, entrainment of clay units by particulate flow results in partial to nearly complete damming of regional groundwater against the fault. Consequences of this damming are discussed further in the text. (C) Distributed particulate flow gives way to localized deformation in discrete crosscutting deformation bands, small-displacement faults, calcite veins, extension fractures, and lens-like cleavage.

numerous parameters in the attenuation of clay and clay-sand mixtures was investigated. The major parameters tested include applied normal stress (6–500 kPa), strain rate (~3–0.3 h per 360 degrees of rotation), sample composition (varying percentages of illite, smectite, kaolin, quartz, feldspar, calcite, and other common rock-forming minerals), and water content (5%–13% above ambient). The experimental results indicate that water content was among the most important controls on the ability of clays to attenuate—a clay source of a given thickness could attenuate to a length that was many times the original thickness when water saturated (Clausen and Gabrielsen, 2002). Based on these experimental results and our observations, we conclude that the pervasive clay-rich fault core of the San Ysidro fault, within the otherwise predominantly siliciclastic protolith, resulted from entrainment during shear accompanied by extreme attenuation of a few protolith clay beds, consistent with deformation in the saturated state. We infer that other structures described earlier by Petit and Laville (1987) also record this saturated state.

Mineralogical and geochemical analyses of fault zone components are generally consistent with water-saturated soft-sediment deformation. Specifically, the chemical signatures of sediments within and outside the fault zone are broadly similar, indicative of a lack of extensive geochemical reactions. Three exceptions are worth noting. First, preferentially calcite-cemented mixed zone sands show notably (and not surprisingly) higher Ca content than uncemented protolith sands. Second, fault core samples that are relatively pure clay have a locally higher clay content than the two protolith clay beds sampled, and they have distinctly higher smectite, Fe, Mg, and, in some cases, illite and K concentrations. These fault core clays may record the entrainment and thus "sampling" of distinct protolith clay layers that are more clay-rich, and compositionally different, from the two studied here. Alternatively, they may record additional processes of clay enrichment directly within the fault core. Two processes, for which evidence was presented previously by Wilson et al. (2006), that might apply here are (1) in situ alteration of unstable grains (most likely lithic fragments or plagioclase) and (2) translocation of clay from the surface through the unsaturated zone. REE data from the San Ysidro fault require that if translocation were important, the source clay would be similar to the protolith layers sampled. Distinguishing unequivocally between these possibilities would require analysis of a wider range of protolith clays, which was prohibited by lack of exposure. Third, samples of the fault core that are clay-sand mixtures tend to show local decreases in concentrations of all elements except potassium relative to the protolith clays. This decrease is most likely indicative of "dilution" of these mixed samples by quartz and feldspar-rich sediment. Support for this interpretation comes from the observation that the mixed samples are generally intermediate in composition between the clay- and sand-rich protoliths, consistent with mechanical mixing, probably by particulate flow.

Collectively, the observations and data presented suggest that the San Ysidro fault zone

structure was determined fundamentally by mechanical processes dictated by both the poorly lithified nature of protolith sediments and probable water saturation. Clay enrichment of the fault core beyond what was physically entrained, if it occurred at all, was a secondary process that most likely involved in situ alteration of mineralogically unstable grains. Such alteration would be facilitated by groundwater saturation of the clay-rich core, which would provide both water content and a substrate for new clay growth.

The development of a virtually continuous, low permeability, clay-rich fault core has important consequences for the permeability evolution of the fault zone and the siliciclastic aquifer in which it resides. In particular, in the absence of effects from crosscutting joints, it is expected to dam cross-fault flow, creating a head drop across the fault (Haneberg, 1995) and thus anisotropy in the regional groundwater flow field due to flow being redirected at the fault (e.g., Fig. 11). Evidence of this type of fault zone acting as a partial barrier is observed today along several faults in basins of the Rio Grande Rift. This evidence includes: hydraulic head drops on the down-gradient side of faults (Johnson and Frost, 2004), interferometric synthetic aperture radar (InSAR) data indicating possible areas of ground surface subsidence and uplift, localized near municipal wells, that appear bounded and controlled by faults (Heywood et al., 2002), and various thermal and geochemical anomalies in the vicinity of faults (Reiter, 1999; Plummer et al., 2004). The details of groundwater (or other fluids) flow directions and magnitudes in the vicinity of such faults are determined by the development of low-permeability fault zone elements (i.e., clays and cements) and their continuity, juxtaposition of sedimentary beds of different permeability on either side of the fault, as well as the magnitude and direction of the regional groundwater flow gradient relative to the fault orientation.

Fault-controlled paleo–groundwater flow is recorded by zones of preferential and asymmetric cementation within the fault zone, consistent with observations in several basins of the Rio Grande Rift (Minor and Hudson, 2006). Some of these zones may include oriented concretions that provide a record of paleoflow direction (cf. Mozley and Goodwin, 1995). Cementation occurred subsequent to fault initiation, and cemented zones themselves show evidence of subsequent fault-related deformation. The latter is not extensive, probably because subsequent slip was localized in weaker elements of the fault zone, such as the fault core, as evidenced by small faults without cements within the clay-rich core itself.

CONCLUSIONS AND IMPLICATIONS

Although the San Ysidro fault exhibits outcrop- to map-scale (1:24,000) geometric and structural features that are similar to those present in faults formed in fully lithified rocks, there are numerous differences. Like some faults in rock (e.g., Scholz, 1987; Hull, 1988; Wibberley et al., 2008), there is no systematic variation in the width of fault zone components (core, mixed zone, or damage zone) with respect to displacement, position along strike, or location within the sedimentary section. One architectural component found in the San Ysidro fault zone that has not been reported in well-lithified rock is a mixed zone (cf. Heynekamp et al., 1999; Rawling and Goodwin, 2003). The San Ysidro mixed zone is a distinctive zone with a notable absence of evidence for fracturing in its initial formation. This zone shows extreme thinning of sand beds indicative of physical entrainment into the fault facilitated by particulate flow, as postulated for the Sand Hill fault (Heynekamp et al., 1999; Rawling and Goodwin, 2003).

Several detailed studies have reported fault-related macroscopic and microscopic structural features in poorly lithified sediments similar to those found in the San Ysidro fault (e.g., Lindsay et al., 1993; Lehner and Pilaar, 1997; Heynekamp et al., 1999; Aydin and Eyal, 2002; Doughty, 2003; Rawling and Goodwin, 2003, 2006; Minor and Hudson, 2006). These observations imply that fluid involvement, and the associated evolution of deformation mechanisms in the growth of faults such as those inferred for the San Ysidro fault, may be common in faulted, poorly lithified sediments in general. Specifically, several of the structures found in the mixed zones and clay-rich fault core of the San Ysidro fault are consistent with the initial stages of deformation having been accommodated in part by particulate flow, at less than ~1 km depth, and below the paleo–water table. The distinct, nearly continuous core of the San Ysidro fault zone is clay-rich virtually everywhere it is observed along its entire 10-km-long exposure in spite of the dominantly siliciclastic protolith. The continuity of clay units in the core of the San Ysidro fault zone may be a natural analog for the clay smear experiments by Clausen and Gabrielsen (2002). In these experiments, water content was determined to be the most critical experimental parameter allowing clay units to be attenuated to lengths many times their original thickness, an observation conceptually consistent with at least the initial inferred formation of the San Ysidro fault core in a groundwater-saturated state. Subsequent minor deformation was accommodated by discrete structures such as crosscutting sparry calcite veins, joints, and small-displacement faults, suggesting that the sediments eventually became stiff enough to support fracturing in fluid-saturated media as the fault evolved (cf. Rawling and Goodwin, 2006). Alternatively, Cashman et al. (2007) have shown that creep can be accommodated by particulate flow and coseismic slip by deformation bands in faulted, unlithified sands above creeping versus seismically active segments of the San Andreas fault. Thus, the transition in deformation style in the San Ysidro fault from distributed particulate flow to formation of localized deformation bands could reflect compaction and (or) digenetic (i.e., cement-related) stiffening of the sediments, and (or) a change from creep to seismic strain rates.

As with faults in rock, the clay-rich core of the San Ysidro fault zone is a structural and lithologic heterogeneity within its protolith. However, the formation of the core in the San Ysidro fault zone may be indicative of dominantly mechanical processes in contrast to the dominantly geochemical or combined mechanical-geochemical processes reported for the formation of clay-rich fault cores in fully lithified rock (e.g., Lovering, 1942; Sibson, 1977; Bruhn et al., 1990; Goddard and Evans, 1995; Hitzman, 1999; Yonkee and Parry, 2001; Eichhubl et al., 2005). We infer that the low-permeability, clay-rich fault core became part of the San Ysidro fault zone predominantly by mechanical entrainment and extreme attenuation of a few protolith clay-rich beds controlled by particulate flow in groundwater-saturated materials with little change in geochemistry or permeability. In contrast, clay-rich fault cores in rock commonly form by pervasive, permeability-enhancing brittle fracture and cataclasis of the protolith with attendant mineralogical and (or) geochemical change.

Once the relatively low-permeability clay-rich fault core was formed along much of the length of the fault zone, we infer that the San Ysidro became a partial barrier to groundwater flow and thus, potentially, the boundary of a fault compartment. Given the relatively high permeability contrast between the protolith (as high as 6.8×10^{-12} m^2) and clay-rich fault core (as low as 3.0×10^{-20} m^2), and the significant spatial continuity of each low-permeability fault zone architectural component, it is clear that faults in poorly lithified sediments might impede modern cross-fault groundwater flow and promote anisotropic, along-fault flow (cf. Caine and Forster, 1999; Rawling et al., 2001). Although the clay-rich core of the San Ysidro fault is laterally persistent along strike, its thickness is variable, and it pinches out in a few isolated locations. It is the low-permeability features in this type of system that will throttle down groundwater flow across faults (Bredehoeft et al., 1992; Haneberg, 1995; Heynekamp et al., 1999).

Thus, identification of the size and location of relatively high-permeability "hydraulic holes" in such faults is among the key geological factors to better understanding the extent that faulting may compartmentalize an aquifer or, for that matter, a hydrocarbon reservoir. Other important factors for such compartmentalization include the locations of low-permeability confining units and the three-dimensional geometry of the faulted sedimentary sequence, the number of faults, their lengths, and types of linkages between them.

An important finding from the aeromagnetic surveys of Grauch et al. (2001) is that the basins of the Rio Grande Rift appear to have many more buried, long, and continuous faults than have been mapped at the surface. If such faults formed by processes similar to those we have inferred for the San Ysidro fault, resulting in pervasive clay-rich and calcite-cemented fault cores and mixed zones, these types of faults could compartmentalize the basin-fill aquifers of the Rio Grande Rift to a greater extent than is currently realized. Compartmentalization may be exacerbated as pumping stresses on the aquifer system increase due to increased demand for groundwater from population growth and if the climate in the southwestern United States becomes more arid—a likely possibility due to global warming (Sheppard et al., 2002; Englehart and Douglas, 2003).

ACKNOWLEDGMENTS

This work was funded by the U.S. Geological Survey, Geologic Discipline, National Cooperative Geologic Mapping and Mineral Resources Programs under the Geologic Framework of Rio Grande Basins Project. We are grateful to Peter Pino of the Zia Pueblo, New Mexico, who granted access to the field area. Discussions with Tien Grauch, Mark Hudson, Dan Koning, and Sean Connell were instrumental in germination of ideas related to this work. Dennis Eberl and Steve Sutley of the U.S. Geological Survey are thanked for providing X-ray diffraction analyses for this study. George Breit, Peter Eichhubl, Chris Potter, Geoffrey Rawling, and Jennifer Wilson provided constructive peer reviews, and we thank them for their conscientious efforts. Laurel Goodwin provided exceptional editorial guidance that greatly improved the clarity of the paper.

REFERENCES CITED

Anders, E., and Ebihara, M., 1982, Solar-system abundances of the elements: Geochimica et Cosmochimica Acta, v. 46, p. 2363–2380, doi: 10.1016/0016-7037(82)90208-3.

Antonellini, M., and Aydin, A., 1994, Effect of faulting on fluid flow in porous sandstones: Petrophysical properties: American Association of Petroleum Geologists Bulletin, v. 78, p. 355–377.

Aydin, A., and Eyal, Y., 2002, Anatomy of a normal fault with shale smear: Implications for fault seal: American Association of Petroleum Geologists Bulletin, v. 86, p. 1367–1381.

Aydin, A., and Johnson, A.M., 1978, Development of faults as zones of deformation bands and as slip surfaces in sandstone; rock friction and earthquake prediction: Pure and Applied Geophysics, v. 116, p. 931–942, doi: 10.1007/BF00876547.

Bense, V.F., Van den Berg, E.H., and Van Balen, R.T., 2003, Deformation mechanisms and hydraulic properties of fault zones in unconsolidated sediments; the Roer Valley Rift system, The Netherlands: Hydrogeology Journal, v. 11, p. 319–332.

Bredehoeft, J.D., Belitz, K., and Sharp-Hansen, S., 1992, The hydrodynamics of the Big Horn Basin: A study of the role of faults: American Association of Petroleum Geologists Bulletin, v. 76, p. 530–546.

Briggs, P.H., and Meier, A.L., 2002, The determination of forty-two elements in geological materials by inductively coupled plasma–mass spectrometry, *in* Taggart, J.E., ed., Analytical Methods for Chemical Analysis of Geologic and Other Materials: U.S. Geological Survey Open-File Report 02–223, p. I1–I14 (http://pubs.usgs.gov/of/2002/ofr-02-0223/).

Bruhn, R.L., Yonkee, W.E., and Parry, W.T., 1990, Structural and fluid-chemical properties of seismogenic normal faults: Tectonophysics, v. 175, p. 139–157, doi: 10.1016/0040-1951(90)90135-U.

Caine, J.S., and Forster, C.B., 1999, Fault zone architecture and fluid flow: Insights from field data and numerical modeling, *in* Haneberg, W.C., Mozley, P.S., Moore, J.C, and Goodwin, L.B., eds., Faults and Sub-Surface Fluid Flow in the Shallow Crust: American Geophysical Union Geophysical Monograph 113, p. 101–127.

Caine, J.S., Evans, J.P., and Forster, C.B., 1996, Fault zone architecture and permeability structure: Geology, v. 24, p. 1025–1028, doi: 10.1130/0091-7613(1996)024<1025:FZAAPS>2.3.CO;2.

Cashman, S.M., Baldwin, J.N., Cashman, K.V., Swanson, K., and Crawford, R., 2007, Microstructures developed by coseismic and aseismic faulting in near-surface sediments, San Andreas fault, California: Geology, v. 35, p. 611–614, doi: 10.1130/G23545A.1.

Cather, S.M., Connell, S.D., Heynekamp, M.R., and Goodwin, L.B., 1997, Geology of the Arroyo de las Calabacillas (Sky Village SE) 7.5 Minute quadrangle, Sandoval County, New Mexico: Socorro, New Mexico, New Mexico Bureau of Mines and Mineral Resources Open-File Geologic Map 9, scale 1:24,000.

Chapin, C.E., and Cather, S.M., 1994, Tectonic setting of the axial basins of the northern and central Rio Grande Rift, *in* Keller, G.R., and Cather, S.M., eds., Basins of the Rio Grande Rift—Structure, Stratigraphy, and Tectonic Setting: Geological Society of America Special Paper 291, p. 5–25.

Chester, F.M., and Logan, J.M., 1986, Implications for mechanical properties of brittle faults from observations of the Punchbowl fault zone, California: Pure and Applied Geophysics, v. 124, p. 79–106, doi: 10.1007/BF00875720.

Childs, C., Watterson, J., and Walsh, J.J., 1996, A model for the structure and development of fault zones: Journal of the Geological Society of London, v. 153, p. 337–340, doi: 10.1144/gsjgs.153.3.0337.

Clausen, J.A., and Gabrielsen, R.H., 2002, Parameters that control the development of clay smear at low stress states; an experimental study using ring-shear apparatus: Journal of Structural Geology, v. 24, p. 1569–1586, doi: 10.1016/S0191-8141(01)00157-2.

Connell, S.D., 2006, Preliminary Geologic Map of the Albuquerque–Rio Rancho Metropolitan Area & Vicinity, Bernalillo and Sandoval Counties, New Mexico: New Mexico Bureau of Geology and Mineral Resources: U.S. Geological Survey Open-File Report 496, 2 plates, scale 1:50,000.

Connell, S.D., Koning, D.J., and Cather, S.M., 1999, Revisions to the stratigraphic nomenclature of the Santa Fe Group, northwestern Albuquerque Basin, New Mexico, *in* Pazzaglia, F.J., and Lucas, S.G., eds., Albuquerque Geology: New Mexico Geological Society Guidebook, v. 50, p. 337–353.

Doughty, P.T., 2003, Clay smear seals and fault sealing potential of an exhumed growth fault, Rio Grande Rift, New Mexico: Fault seals: American Association of Petroleum Geologists Bulletin, v. 87, p. 427–444.

Eberl, D.D., 2003, User Guide to RockJock—A Program for Determining Quantitative Mineralogy from X-Ray Diffraction Data: U.S. Geological Survey Open File Report 03–78, 40 p. (ftp://brrcrftp.cr.usgs.gov/pub/ddeberl/RockJock).

Egholm, D.G., Clausen, O.R., Sandiford, M., Kristensen, M.B., and Korstgård, J.A., 2008, The mechanics of clay smearing along faults: Geology, v. 36, p. 787–790, doi: 10.1130/G24975A.1.

Eichhubl, P., D'Onfro, P.S., Aydin, A., Waters, J., and McCarty, D.K., 2005, Structure, petrophysics, and diagenesis of shale entrained along a normal fault at Black Diamond Mines, California—Implications for fault seal: American Association of Petroleum Geologists Bulletin, v. 89, p. 1113–1137.

Engelder, J.T., 1974, Cataclasis and the generation of fault gouge: Geological Society of America Bulletin, v. 85, p. 1515–1522, doi: 10.1130/0016-7606(1974)85<1515:CATGOF>2.0.CO;2.

Englehart, P.J., and Douglas, A.V., 2003, Urbanization and seasonal temperature trends: Observational evidence from a data-sparse part of North America: International Journal of Climatology, v. 23, p. 1253–1263, doi: 10.1002/joc.935.

Goddard, J.V., and Evans, J.P., 1995, Chemical changes and fluid-rock interaction in faults of crystalline thrust sheets, northwestern Wyoming, U.S.A.: Journal of Structural Geology, v. 17, p. 533–547, doi: 10.1016/0191-8141(94)00068-B.

Grauch, V.J.S., Gillespie, C.L., and Keller, G.R., 1999, Discussion of new gravity maps for the Albuquerque Basin area, *in* Pazzaglia, F.J., and Lucas, S.G., eds., Albuquerque Geology: New Mexico Geological Society Guidebook 50, p. 119–124.

Grauch, V.J.S., Hudson, M.R., and Minor, S.A., 2001, Aeromagnetic expression of faults that offset basin fill, Albuquerque Basin, New Mexico: Geophysics, v. 66, p. 707–720, doi: 10.1190/1.1444961.

Grauch, V.J.S., Hudson, M.R., Minor, S.A., and Caine, J.S., 2006, Sources of along-strike variation in magnetic anomalies related to intrasedimentary faults: A case study from the Rio Grande Rift, USA: Exploration Geophysics, v. 37, p. 372–378, doi: 10.1071/EG06372.

Haneberg, W.C., 1995, Steady state groundwater flow across idealized faults: Water Resources Research, v. 31, p. 1815–1820, doi: 10.1029/95WR01178.

Hawley, J.W., Haase, C.S., and Lozinsky, R.P., 1995, An underground view of the Albuquerque Basin, *in* Ortega-Klett, C.T., ed., The Water Future of Albuquerque and the Middle Rio Grande Basin: New Mexico Water Resources Research Institute Report 290, p. 37–55.

Heynekamp, M.R., Goodwin, L.B., Mozley, P.S., and Haneberg, W.C., 1999, Controls on fault zone architecture in poorly lithified sediments, Rio Grande Rift, New Mexico: Implications for fault zone permeability and fluid flow, *in* Haneberg, W.C., Mozley, P.S., Moore, J.C., and Goodwin, L.B., eds., Faults and Sub-Surface Fluid Flow in the Shallow Crust: American Geophysical Union Geophysical Monograph 113, p. 27–49.

Heywood, C.E., Galloway, D.L., and Stork, S.V., 2002, Ground Displacements Caused by Aquifer-System Water-Level Variations Observed Using Interferometric Synthetic Aperture Radar near Albuquerque, New Mexico: U.S. Geological Survey Water-Resources Investigations Report 02–4235, 24 p.

Hitzman, M.W., 1999, Extensional faults that localize Irish syndiagenetic Zn-Pb deposits and their reactivation during Variscan compression, *in* McCaffrey, K.J.W., Lonergan, L., and Wilkinson, J., eds., Fractures, Fluid Flow and Mineralization: Geological Society of London Special Publication 155, p. 233–245.

Hudson, M.R., Grauch, V.J.S., and Minor, S.A., 2008, Rock magnetic characterization of faulted sediments with associated magnetic anomalies in the Albuquerque Basin, Rio Grande Rift, New Mexico: Geological Society of America Bulletin, v. 120, p. 641–658, doi: 10.1130/B26213.1.

Hull, J., 1988, Thickness-displacement relationships for deformation zones: Journal of Structural Geology, v. 10, p. 431–435.

Johnson, P.S., and Frost, J., 2004, Hydrologic conditions in the southeastern Española Basin based on recent data collection near Santa Fe, New Mexico—A view

from midstream, *in* Hudson, M.R., ed., Geologic and Hydrogeologic Framework of the Española Basin–Proceedings of the 3rd Annual Española Basin Workshop, Santa Fe, New Mexico, March 2–3, 2004: U.S. Geological Survey Open-File Report 2004–1093, p. 2.

Kelley, V.C., 1977, Geology of Albuquerque Basin, New Mexico: New Mexico Bureau of Mines and Mineral Resources Memoir 33, 59 p.

Kelley, V.C., 1982, The right-relayed Rio Grande Rift, Taos to Hatch, New Mexico, *in* Grambling, J.A., and Wells, S.G., eds., Albuquerque Country II: New Mexico Geological Society Guidebook 33, p. 147–151.

Kelson, K.I., and Personius, S.F., compilers, 1997, Fault number 2029b, Jemez–San Ysidro fault, San Ysidro section, *in* Quaternary Fault and Fold Database of the United States: http://earthquakes.usgs.gov/regional/qfaults (March 2009).

Knipe, R.J., 1993, The influence of fault zone processes and diagenesis on fluid flow, *in* Horbury, A.D., and Robinson, A.G., eds., Diagenesis and Basin Development: American Association of Petroleum Geologists Studies in Geology 36, p. 135–151.

Koning, D.J., Pederson, J., Pazzaglia, F.J., and Cather, S.M., 1998, Geology of the Cerro Conejo (Sky Village NE) 7.5-Minute Quadrangle, Sandoval County, New Mexico: New Mexico Bureau of Mines and Mineral Resources Open-File Geologic Map GM 45, scale 1:24,000.

Lehner, F.K., and Pilaar, W.F., 1997, The emplacement of clay smears in synsedimentary normal faults: Inferences from field observations near Frenchen, Germany, *in* Møller-Pederson, P., and Koestler, eds., Hydrocarbon Seals: Importance for Exploration and Production: Amsterdam, Elsevier, p. 39–50.

Lindsay, N.G., Murphy, F.C., Walsh, J.J., and Watterson, J., 1993, Outcrop studies of shale smears on fault surfaces, *in* Flint, S.S., and Bryant, I.D., eds., The Geological Modeling of Hydrocarbon Reservoirs and Outcrop Analogs: International Association of Sedimentologists Special Publication 15, p. 113–123.

Lopez, D.L., and Smith, L., 1996, Fluid flow in fault zones: Influence of hydraulic anisotropy and heterogeneity on the fluid flow and heat transfer regime: Water Resources Research, v. 32, p. 3227–3235, doi: 10.1029/96WR02101.

Lovering, T.S., 1942, The mineral belt of the Colorado Front Range, *in* Newhouse, W.H., ed., Ore Deposits as Related to Structural Features: New York, Hafner Publishing, p. 79–93.

Lowe, D.R., 1975, Water escape structures in coarse-grained sediments: Sedimentology, v. 22, p. 157–204, doi: 10.1111/j.1365-3091.1975.tb00290.x.

Martel, S.J., 1990, Formation of compound strike-slip fault zones, Mount Abbot quadrangle, California: Journal of Structural Geology, v. 12, p. 869–882, doi: 10.1016/0191-8141(90)90060-C.

May, S.J., and Russell, L.R., 1994, Thickness of the synrift Santa Fe Group in the Albuquerque Basin and its relation to structural style, *in* Keller, G.R., and Cather, S.M., eds., Basins of the Rio Grande Rift—Structure, Stratigraphy, and Tectonic Setting: Geological Society of America Special Paper 291, p. 113–124.

McCaig, A.M., 1989, Fluid flow through fault zones: Nature, v. 340, p. 600, doi: 10.1038/340600a0.

Means, W.D., 1987, A newly recognized type of slickenside striation: Journal of Structural Geology, v. 9, p. 585–590.

Meier, A.L., and Slowik, T., 2002, Rare earth elements by inductively coupled plasma–mass spectrometry, *in* Taggart, J.E., ed., Analytical Methods for Chemical Analysis of Geologic and Other Materials: U.S. Geological Survey Open-File Report 02–223, p. K1–K8 (http://pubs.usgs.gov/of/2002/ofr-02-0223/).

Minor, S.A., and Hudson, M.R., 2006, Regional Survey of Structural Properties and Cementation Patterns of Fault Zones in the Northern Part of the Albuquerque Basin, New Mexico: Implications for Ground-Water Flow: U.S. Geological Survey Professional Paper 1719, 32 p.

Mozley, P.S., and Goodwin, L.B., 1995, Patterns of cementation along a Cenozoic normal fault; a record of paleoflow orientations: Geology, v. 23, p. 539–542, doi: 10.1130/0091-7613(1995)023<0539:POCAAC>2.3.CO;2.

Mozley, P.S., Rawling, G.C., and Goodwin, L.B., 2004, Controls on fault zone architecture and cementation in poorly consolidated sands and gravels; Loma Blanca fault, Rio Grande Rift, New Mexico: Geological Society of America Abstracts with Programs, v. 36, no. 5, p. 425.

Personius, S.F., Machette, M.N., and Kelson, K.I., 1999, Quaternary faults in the Albuquerque area—An update, *in* Pazzaglia, F.J., and Lucas, S.G., eds., Albuquerque Geology: New Mexico Geological Society Guidebook, v. 50, p. 189–200.

Petit, J., and Laville, E., 1987, Morphology and microstructures of hydroplastic slickensides in sandstone, *in* Jones, M.E., and Preston, M.F., eds., Deformation of Sediments and Sedimentary Rocks: Geological Society of London Special Publication 29, p. 107–121.

Plummer, N.L., Bexfield, L.M., Anderholm, S.K., Sanford, W.E., and Busenberg, E., 2004, Geochemical Characterization of Ground-Water Flow in the Santa Fe Group Aquifer System, Middle Rio Grande Basin, New Mexico: U.S. Geological Survey Water-Resources Investigations Report 2003–4131, 395 p.

Rawling, G.C., and Goodwin, L.B., 2003, Cataclasis and particulate flow in faulted, poorly lithified sediments: Journal of Structural Geology, v. 25, p. 317–331, doi: 10.1016/S0191-8141(02)00041-X.

Rawling, G.C., and Goodwin, L.B., 2006, Structural record of the mechanical evolution of mixed zones in faulted poorly lithified sediments, Rio Grande Rift, New Mexico, USA: Journal of Structural Geology, v. 28, p. 1623–1639, doi: 10.1016/j.jsg.2006.06.008.

Rawling, G.C., Goodwin, L.B., and Wilson, J.L., 2001, Internal architecture, permeability structure, and hydrologic significance of contrasting fault zone types: Geology, v. 29, p. 43–46, doi: 10.1130/0091-7613(2001)029<0043:IAPSAH>2.0.CO;2.

Reiter, M., 1999, Hydrogeothermal studies on the southern part of Sandia National Laboratories/Kirtland Air Force Base—Data regarding ground-water flow across the boundary of an intermontane basin, *in* Haneberg, W.C., Mozley, P.S., Moore, J.C., and Goodwin, L.B., eds., Faults and Sub-Surface Fluid Flow in the Shallow Crust: American Geophysical Union Geophysical Monograph 113, p. 207–222.

Scholz, C.H., 1987, Wear and gouge formation in brittle faulting: Geology, v. 15, p. 493–497, doi: 10.1130/0091-7613(1987)15<493:WAGFIB>2.0.CO;2.

Sheppard, P.R., Comrie, A.C., Packin, G.D., Angersbach, K., and Hughes, M.K., 2002, The climate of the US Southwest: Climate Research, v. 21, p. 219–238, doi: 10.3354/cr021219.

Shipton, Z.K., and Cowie, P.A., 2001, Damage zone and slip-surface evolution over μm to km scales in high-porosity Navajo Sandstone, Utah: Journal of Structural Geology, v. 23, p. 1825–1844, doi: 10.1016/S0191-8141(01)00035-9.

Shipton, Z.K., Evans, J.P., Robeson, K.R., Forster, C.B., and Snelgrove, S., 2002, Structural heterogeneity and permeability in faulted eolian sandstone; implications for subsurface modeling of faults: American Association of Petroleum Geologists Bulletin, v. 86, p. 863–883.

Sibson, R.H., 1977, Fault rocks and fault mechanisms: Journal of the Geological Society of London, v. 133, p. 191–231, doi: 10.1144/gsjgs.133.3.0191.

Sibson, R.H., 1994, Crustal stress, faulting, and fluid flow, *in* Parnell, J., ed., Geofluids: Origin, Migration, and Evolution of Fluids in Sedimentary Basins: Geological Society of London Special Publication 78, p. 69–84, doi: 10.1144/GSL.SP.1994.078.01.07.

Smith, D.K., Johnson, G.G., Jr., Scheible, W., Wims, A.M., Johnson, J.L., and Ullmann, G., 1987, Quantitative X-ray powder diffraction method using the full diffraction pattern: Powder Diffraction, v. 2, p. 73–77.

Smith, G.A., McIntosh, W., and Kuhle, A.J., 2001, Sedimentologic and geomorphic evidence for seesaw subsidence of the Santo Domingo accommodation zone basin, Rio Grande Rift, New Mexico: Geological Society of America Bulletin, v. 113, p. 561–574.

Sweeney, R.E., Grauch, V.J.S., and Phillips, J.D., 2002, Merged Digital Aeromagnetic Data for the Middle Rio Grande and Southern Española Basins, New Mexico: U.S. Geological Survey Open-File Report 02–0205, 15 p.

Taylor, J.C., 1991, Computer programs for the standardless quantitative analysis of minerals using the full powder diffraction profile: Powder Diffraction, v. 6, p. 2–9.

Vrolijk, P., and van der Pluijm, B.A., 1999, Clay gouge: Journal of Structural Geology, v. 21, p. 1039–1048, doi: 10.1016/S0191-8141(99)00103-0.

Weber, K.J., Mandl, G., Pilaar, W.F., Lehner, F., and Precious, R.G., 1978, The role of faults in hydrocarbon migration and trapping in Nigerian growth fault structures: 10th Annual Offshore Technology Conference Proceedings, Houston, Texas: American Institute of Mining, Metallurgical, and Petroleum Engineers, v. 4, p. 2643–2653.

Wibberley, C.A.J., Yielding, G., and Di Toro, G., 2008, Recent advances in the understanding of fault zone internal structure: A review, *in* Wibberley, C.A.J., Kurz, W., Imber, J., Holdsworth, R.E., and Collettini, C., eds., The Internal Structure of Fault Zones: Implications for Mechanical and Fluid-Flow Properties: Geological Society of London Special Publication 299, p. 5–33.

Wilson, J.E., Goodwin, L.B., and Lewis, C., 2006, Diagenesis of deformation band faults: Record and mechanical consequences of vadose zone flow and transport in the Bandelier Tuff, Los Alamos, New Mexico: Journal of Geophysical Research, v. 111, p. B09021, doi:10.1029/2005JB003892.

Woodward, L.A., and Reutschilling, R.L., 1976, Geology of San Ysidro Quadrangle, New Mexico: New Mexico Bureau of Mines and Mineral Resources Geologic Map GM-37, scale 1:24,000.

Yonkee, W.A., and Parry, W.T., 2001, Relations between progressive deformation and fluid-rock interaction during growth of fault and shear zones in a basement-cored thrust sheet, Sevier orogenic belt, Utah, *in* Earth System Processes Meeting Programs with Abstracts: Edinburgh, Scotland, The Geological Society of America and The Geological Society of London, p. 37.

Manuscript Received 8 December 2006
Revised Manuscript Received 25 December 2008
Manuscript Accepted 5 January 2009

Printed in the USA